ISSN : 0974 - 7494 Volume 10 Issue 2

Nano Science and Nano Technology
An Indian Journal

Review

NSNTAIJ, 10(2), 2016 [073-082]

Surface nanostructures in oxides doped with Me/RE ions

N.A.Kulagin
Ukrainian with Germany Joint Venture "Firma SIFA", av. Shakespeare, 6-48, Kharkiv, 61045, (UKRAINE)
E-mail: nkulagin@bestnet.kharkov.ua

ABSTRACT

The results of studying experimental and theoretical results on spectral properties of selected oxides as pure as doped with Me/RE ions discussed this paper. Experimental data resulting from investigation of radiation induced defects in sapphire and strontium titanate over γ- or plasma flow. Ordered and quasi-ordered nano- and sub-nanostructures were discovered on surface of the oxides over plasma flow and performed using high resolution SEM and AFM techniques. Registered ion's X ray line shift shows change in the oxidation state in the host and impurity ions. XRD data were calculated for crystal's crystalline lattice. Ab initio simulation of cluster electronic structure and ions energy level's scheme was taken into account for interpretation.

KEYWORDS

Nanostructure;
Color center;
Defect;
Oxide;
Valence.

INTRODUCTION

Oxide single crystals were and continue to be very interested objects for study and applications. Simple oxide, as sapphire, α-Al_2O_3 or complex one, perovskite as strontium titanate, $SrTiO_3$ (STO), are the best objects for study of electronic structure of single crystals as well as pure or doped ones with ions of transition group elements, so-called Me ions or/and rare earth ions, RE. Growing interest to nano-sized crystals and clusters moves to detail study of the samples before and after treatment.

It is well known[1 – 3] that physical properties of wide band gap oxides depend on type and concentration of doped ions and structural defects. On other hand, properties of the main defects strongly depend on crystal producing technology. Follow[1 - 6] notice that point defects such as oxygen's or cation's vacancies, interstitial ions and impurities play important role in additional optical absorption of natural and grown crystals.

As shown in[1 - 2] pure and doped crystals are growing in different conditions. Moreover, deviation from stoichiometry accompanied by evaporation of oxygen and/or selected oxides in growth chamber, and ground crystal properties may be sufficiently changed upon special thermal treatment in different atmosphere[4 - 6]. Moreover, introduction of impurities leads to appearance of additional point and colour centres and related absorption or luminescence bands[1 - 7].

It is known that ionizing radiation, exemplary, γ -, electron's, etc. affects in change in spectral properties of selected wide band gap crystals and leads to rising additional lines and bands in optical absorption or/and luminescence spectra, including ESR

Review

ones[6 - 7]. The additional optical absorption, so-called AA spectra, observed in different oxides appears through radiation induced colour centres and changes in oxidation state of host and impurity ions[7 - 12]. Recently more complex figures including ordered nano- or sub-nanostuctures were discovered on selected oxide surface over plasma flow[8 - 11].

The results of studying the colour centres producing change in spectral properties of the irradiated oxides, such as optical absorption and luminescence, ESR, thermo-luminescence, TSL, and thermo-conductivity, TSC techniques were performed in detail[6 - 12]. For estimation of ion's oxidation state stability as component as doping ones, the method of valence shift in X ray lines, VSXRL, proposed in[7, 13] were taken into account. Crystalline lattice parameters in the samples were calculated, too. Change in surface morphology was studied with help of high resolution scanning electron, SEM, and atomic force, AFM, microscopy techniques[8, 10 - 11].

Follow[11, 14] the results of theoretical simulation based on the self-consistent field theory for impurity ions and clusters which are closely to experiments for tested oxides are performed.

Setups and samples

Optical spectra of the tested oxides as sapphire and strontium titanate, STO, in the full range of transparency were studied before and after effect of ionizing and plasma flow. Standard optical measurements in VUV - UV, visible and IR region of spectra (T = 300, 77, 10 and 4.2 K), ESR technique (Varian spectrometer, λ = 3 cm, 8 mm, T = 77, 300 K)[2, 5], original TSL -TSC[6, 12 - 13] experiments were involved to study energy and concentration of trapping centers, energy levels schemes of impurities and point defects.

Original VSXRL method was developed of studying the oxidation state of host and impurity ions (energy-dispersive X ray line spectroscopy, EDX technique) with help of modified microanalyser Cameca[11 - 14]. Atomic force microscopy (AFM, NP 206), scanning electron microscopy (SEM, JEOL 840A) were used to study sample's surface. Additionally, SEM images were studied in TU Dresden with help of Zeiss ULTRA5 (thermal Schottky field emitter) technique including cathode luminescence emission spectra device.

Follow[6, 9 - 12] change in crystals growth technology and related variation in spectral properties of the samples grown under different conditions was studied. Application of the samples obtained from charges of different quality and variation in crystal growth parameters (atmosphere, temperature, etc.) in growing chamber or/and additional thermal treatment has been used, too[6, 19 - 21]. Selected crystals contain of doped and co-doped Me/RE ions: Ti, V, Cr, Mn, Fe, Pr, Nd, etc.

Pure and un-doped sapphires were prepared by the main method such as: Verneuil - V, Czochralsky - Cz, Stemanov - S, vertical/horizontal direction – DC, etc. ones. Selected crystals were grown from super pure charges, exemplary - V_{sp}, DC_{sp}, etc. Doped crystals, as ruby, α-Al_2O_3: Cr, with Cr ion concentration up 10^{-3} to $5 \cdot 10^{-1}$ wt % and sapphire doped with other Me ions were grown by Verneuil technique and vertical/horizontal direction method using the standard and super pure mixture. Additional information for sapphire crystals growth techniques discussed in[6, 14, 22].

STO samples were created by Verneuil and Czochralsky techniques using super perfect and standard charge and, sometimes, deeply changing growth conditions. Crystal growth techniques for STO single crystals were discussed in[10 - 11, 22, 24], too.

The results of studying the crystalline lattice of the samples were performed with help of diffractometer DRON-3UM for crystals and power samples and described in detail in[10, 15].

Surface of the plasma treated samples

Plasma treatment of the oxide surfaces was carried out with help of the two different magneto-plasma compressors (MPC). A detailed description of experimental setups and methods may be found in[26 - 27]. Briefly, the MPC is a single-stage quasi-stationary plasma accelerator. The self-magnetic-ûeld-sample shielding of an anode rods diminishes level of erosion. Anode rods are connected by a carrier, which enables MPC flux magnitude in order of magnitude of 10^{23} $cm^{-2} \cdot s^{-1}$ and energy values of W = 1, 5, 10, 15 and 20 $J \cdot cm^{-2}$ per impulse for different

devices, respectively.

Corresponding time for quasi-stable state plasma impulse in different MPC varied in range: $\tau = (1 - 150)\cdot 10^{-6}$ s. Estimated maximum of a local temperature *T* on the sample surface is near T ~ 2000 K[18]. The thickness of the near-surface layer involved by plasma-treatment according to ellipsometry measurement, recorded by Prof. A. Konstantinova, is nearby 10^{-6} - 10^{-7} m. SEM and AFM images of the crystal surfaces in original state are similar for the pure and doped samples.

Exemplary, SEM and AFM images of selected area on the STO: Nd surface sample, perfect sapphire and ruby one created by different MPC devices mentioned above plasma-flow with the energy density (dose) of about W = 1 - 15 J·cm^{-2} given in Figures 1- 4. Follow[10-11] the image (Figure 1) was created by "short time" high intensive plasma impulse. As was note above, the image (Figures 2 - 4) corresponds to a "long time"middle energy plasma impulse[25 - 26].

Nanostructures appearing on the STO surface consist of ordered or quasi-ordered system of unit pyramid type crystallites with size of about 10^{-7} – 10^{-10} m (Figures 1 and 2). Different images including one- or two level nano-structures were recorded for selected sample's place because of radial distribution in plasma energy flow. Two-level ordered nanostructures were discovered and studied on the surface of main part of the STO samples. Selected areas including quasi-ordered system of needle-like crystallites with size of about 10^{-8} - 10^{-10} m were founded on sapphire surface (Figure 3) and additionally treated in reducing atmosphere ruby sample (Figure 4).

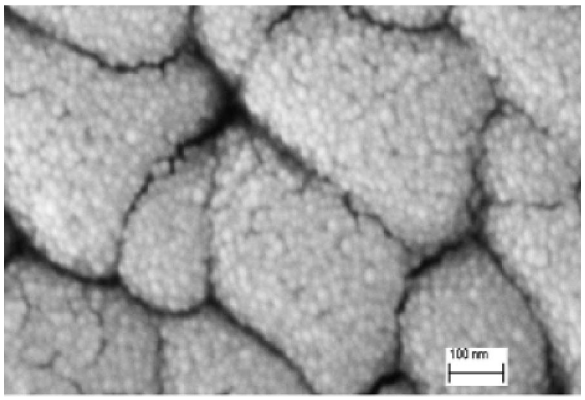

Figure 1 : SEM image of STO: Nd sample over plasma flow

Figure 2 : AFM image of STO: Nd sample over plasma flow

Optics and XRD

Follow[10 - 14] we are waiting for strong dependence of plasma flow effect on crystal growth conditions and investigate selected spectral properties of sapphire and STO samples as pure and doped ones growing under different conditions are the following.

Sapphire

Optical absorption spectra in the pure sapphire

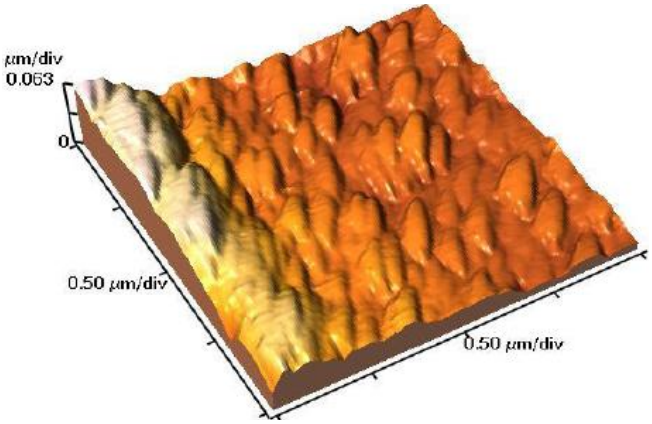

Figure 3 : AFM image of STO: Sm sample over plasma flow

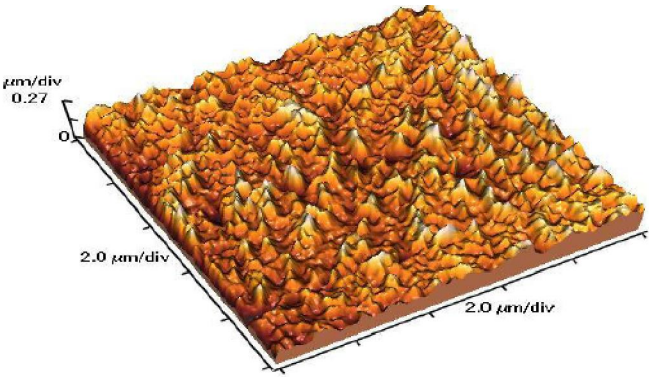

Figure 4 : AFM image of ruby sample over plasma flow and additional treatment

Review

grown with different methods were performed in[6, 12 - 14]. Fundamental absorption edge for the perfect samples is nearby λ = 142 nm. Strong optical absorption of nominally pure (un-doped) samples begins at λ = 195 nm and relates to accidental impurities and structural point defects. Selected data for optical, ESR, TSC and TSL spectra in super pure sapphire are given in[6].

Optical absorption bands upon irradiation for the perfect sapphire are absent. For the most of tested and irradiated samples additional absorption, AA, spectra were found. Iradiation of the sapphire containing impurity with small concentration, $C_{imp} < 10^{-2}$ wt %, changes in initial optical bands intensity, only. Rising impurity concentration affects in appearance of intensive AA and diminishing point defects absorption[12 - 13]. And follow[7, 23] we can confirm that concentration of accidental impurities and growth conditions determine profile of point color centers in the sapphire (oxides). AA bands intensity grows with radiation dose and stops under $W = 10^4$ Gy for any type of radiation. As shown in[14, 22- 24] irradiation of pure or doped sapphire stimulated growing conductivity of the samples at 4 orders as much.

Variation in concentration of doped ions and doze of irradiation inducing defects in sapphire was determined with help of ESR technique. Follow[4] the concentration of Cr^{+3} (as mark presenting as accidental impurity for the most samples) may be evaluated via the intensity of ½ ↔ -½ ESR line while total concentration of defects was estimated via the half-width of 3/2 ↔ 1/2 transition in Cr^{+3} ion. Corresponding data for sapphire doped with other Me ions discussed in[11, 14]. Studying optical spectra the sapphire doped with Me ions diminishing role of point defect influence when impurity concentration increasing up 10^{-2} to 0.5 wt % was revealed.

The following AA wide bands peaked at λ = 217, 270, 360 and 460 nm set in irradiated ruby. As shown in[1, 14, 22 – 24] three bands correspond to electron transition in Cr^{+4} ions located in octahedral site of sapphire lattice. Additional data for ions oxidation state and radiation stimulated colour centres in sapphire doped with Me ions were performed in[6 - 7, 21 - 22].

Plasma flow affects in rising scattering light intensity from the pure sapphire and appearance small intensity absorption bands peaked at λ = 217, 270, 360 and 460 nm in ruby ones.

Follow[15, 17] no diffraction peaks in sapphire or ruby treated by plasma flow from crystal surface were recorded.

Strontium titanate

Follow[24, 27 - 29] optical absorption spectra of the STO samples strongly depend on stocihiometry composition and crystals growth conditions. Selected large samples consist of three radial parts: transparent (external), yellow (mid) and "blue spot" (inside) ones wit corresponding absorption spectra including wide bands peaked at λ = 430, 520 nm and additional band peaked at λ = 620 nm in selected samples. Absorption and luminescence spectra in perfect crystals have no bands or lines. The standard samples, including accidental impurity (Cr, Fe, etc.) with concentration $C_{imp} \sim 10^{-2}$ wt % consist of wide bands peaked at λ = 430, 520 nm. Changing in wide spread relative intensity bands was recorded in the un-doped STO samples grown under special conditions.

Follow[15 – 16] optical luminescence band excited by laser's irradiation with λ = 578.2 nm were fitted at λ = 650 nm for the next samples: near stoichiometric relation pure sample, "blue spot" and doped with RE ions. Optical luminescence spectra were recorded in "blue spot" and STO: Mn samples as before as after thermal treatment at T = 77 K during 600 s.

Common picture including laser exciting beam peaking at λ = 578.2 nm, Raman's scattering line rising at 602 nm and wide luminescence band peaked at 650 nm given in Figure 5. Curves 1 and 3 correspond to "blue spot" and STO: Mn samples in original state. Follow[15] curve 2 corresponds to luminescence band in "blue spot" sample after low temperature, T = 77 K, treatment and curve - 4 shows the luminescence band in the STO: Mn plasma treated sample. Note, the luminescence band intensity is in opposite to the absorption intensity one peaking at λ = 620 nm.

Follow[14, 16] during the electron microscopy

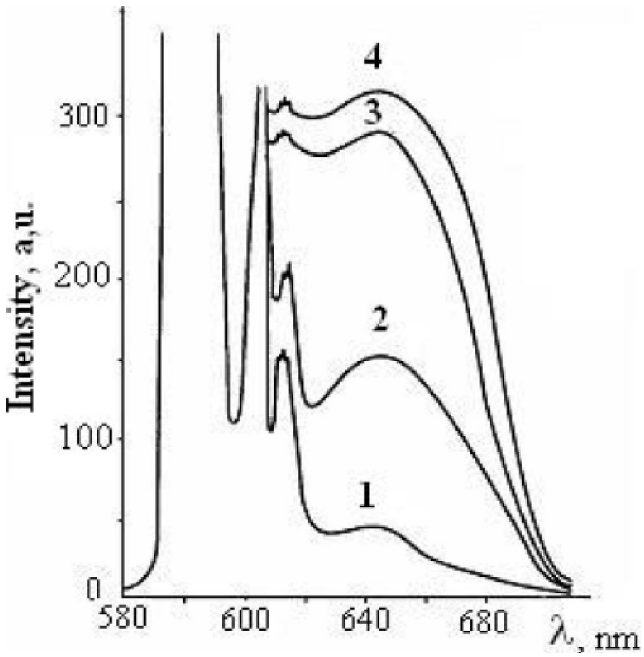

Figure 5 : Spectra of luminescence of perfect sample and doped with $SrTiO_3$: Mn, 1 - before and 2- after thermal treatment at T = 77 K. "Blue spot" sample 3 - before and 4 - over plasma treatment

studying the cathode luminescence spectra in the transparent, yellow and "blue spot" STO sample's parts were recorded under different electron current density (Figures 6 and 7) The intensity ratio for the bands, recorded during probing of the transparent, yellow and blue color regions (Figure 6) peaked at λ = 460, 550, 600 and 700 nm are, respectively: 1/2.35/3.82, 1/3.5/6.25, 1/5.1/7.2 and /6/12. The next data for the bands intensity were recorded: 1.41/ 1.25/1, 7/11/1 and 1/4/2. For the last bands intensity peaked at λ = 550 nm the ratio is following: 1.5/8/1. Order of relative band intensity as 1-2-3 curves peaked at λ = 460 nm, 2-3-1 at λ = 600 nm and small intensity fail at λ = 700 nm (Figure 6) changes to 3-2-1 one fixed at λ = 460 nm, λ = 550 or 600 nm and gigantic intensity peak at λ = 700 nm for yellow crystal (Figure 7).

Follow[14] the ground properties in the STO samples such as: impurity's concentration, C_{imp}, ε_r value, relative stoichiometry relation, Sr/Ti, and concentration of Ti^{+3} ions were recorded. No AA bands or peaks in the STO: Me/RE samples upon γ-irradiation. Strong radiation resistance in pure and doped samples may be explained by relative high conductivity. Dielectric constant in the STO perfect

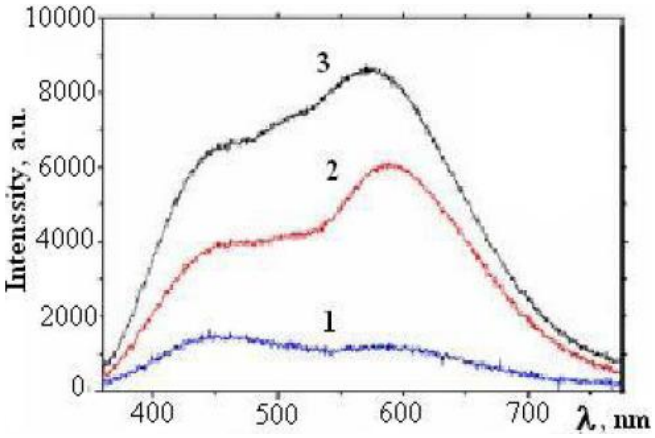

Figure 6 : Cathode luminescence spectra for $SrTiO_3$: 1 - transparent area, 2 - yellow area, 3 - "blue spot" - 3. Conditions 1

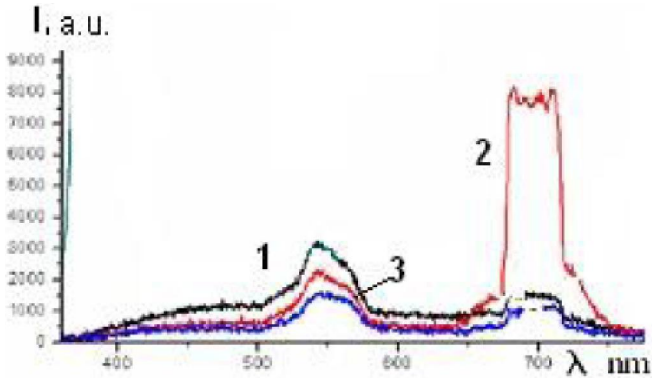

Figure 7 : Cathode luminescence spectra for $SrTiO_3$: 1 - transparent area, 2 - yellow area, 3 - "blue spot" - 3. Conditions 2.

is near ε_r = (320 ± 5) and strongly decreasing for doped samples.

X ray diffraction were studied for perfect, undoped complex sample (consist of transparent, "yellow", "blue spot" parts) and doped with Mn, Co and Nd ions crystals, too. Crystallographic parameter in perfect crystal equals: a = (3.9048 ± 0.0008) Å and a = (3.9038 ± 0.0008) Å for transparent part of the complex sample. Crystallographic parameter in the "yellow" crystal in cubic symmetry was found: a = (3.9032 ± 0.0008) Å.

Follow[14-15] sufficient change in crystallographic symmetry and parameters in the "blue spot" samples were discovered. Tetrahedral system with diffraction peaks under following directions: (100), (110), (111), (200), 210) and (211) and 2Θ = 22.767; 32.391; 39.958; 46.500, 52.375 and 57.839^0, accordingly, were recorded. Corresponding data for crystallographic parameters were found: a = (3.9023 ±

Review

0.0011) Å and c = (5.5213 ± 0.0013) Å. Elementary unit value changes from 59.47 to 84.08 Å^3.

Report[21] shows the parameter a in STO: Nd samples over plasma flow decreases to a = (3.8922± 0.0006) Å when crystallographic lattice symmetry don't change. In the crystals doped with Mn or Co ions cubic symmetry were recorded under room temperature, too. Calculated parameter a in the samples doped with Mn ions changes to a = (3.9045 ± 0.0005) Å and a = (3.9038±0.0005) Å (STO: Co). Tetrahedral lattice symmetry was founded in special grown STO: Fe: V sample under parameters: a = (3.9027 ± 0.0011) Å and c = (5.5218 ± 0.0013) Å.

Follow[15, 18] diminishing crystalline cubic parameter up a = (3.9052 ± 0.0008) Å to a = (3.8922± 0.0006) Å for STO perfect sample and a = (3.8890± 0.0006) Å for STO: Nd was recorded before and after plasma treatment.

Oxidation state of the Me/RE ions

Ti ions in STO

As was noted above, the VSXRL method is based on the dependence of the energies of *K*- *L*-, and other X ray characteristic lines on the ion oxidation state. Studying the change in energy position of Me/RE X ray line the valence of component or impurity ions in oxide upon irradiation, thermal or plasma treatment using X ray lines spectroscopy can be recorded.

Follow[2, 12, 15] accuracy in energy determination in Me$K_{\alpha 1}$ line can be ab initio calculated as difference in energy of n'l'$^{-1}$3d^N configurations with n'l' = 1s or 2p (Me$K_{\alpha 1}$ line) excited electrons, which provides theoretical energy value for Cr$K_{\alpha 1}$ line: E($K_{\alpha 1}$) = 5412.14 eV, when experimental data for Cr metallic equals E($K_{\alpha 1}$) = 5411.88 eV. Valence shift, VS, in X ray line determined as change in X ray line energy related to variation in ion oxidation state[1, 13 - 14]. Selected experimental profiles for Ti$K_{\alpha 1}$ line in STO samples are given in Figure 8. Curve 1 corresponds to Ti$K_{\alpha 1}$ line in perfect crystal, 2 - original $SrTiO_3$: Nd one. Notice, profile for Ti$K_{\alpha 1}$ line in "blue spot" is nearby to curve 2. Curve 3 represents Ti$K_{\alpha 1}$ line profile for STO: Nd sample over plasma flow (doze of about W = 20 J·cm^{-2}). According to theoretical and experimental data the shift in Ti$K_{\alpha 1}$ line indicates change in oxidation state of some part of Ti ions. The positive shift in position of Ti$K_{\alpha 1}$ line in each sample was fixed. Consequently change in Ti ion oxidation state as $Ti^{+4} \rightarrow Ti^{+3}$ transition exactly registered with definite concentration.

Calculated data for VS in Ti$K_{\alpha 1}$ line described by Lorentz function are the following: VS(Ti$K_{\alpha 1}$) = + (0.49 ± 0.09) eV in "blue spot" sample and STO: Nd. VS(Ti$K_{\alpha 1}$) = + (0.37 ± 0.09) eV in STO: Mn. For Ti$K_{\alpha 1}$ line in STO: Nd before and over plasma flow the VS value is following: ΔE(Ti$K_{\alpha 1}$) = + (0.29 ± 0.09) eV. Selected data for other tested samples are similar: VS(Ti $K_{\alpha 1}$) = +(0.32 ± 0.09) eV, STO: Ni (Co) and VS(Ti$K_{\alpha 1}$) = + (0.45 ± 0.09) eV äëÿ STO: Sm.

Positive shift in the energy of Ti$K_{\alpha 1}$ X ray line strongly correlates with intensity of AA bands in STO

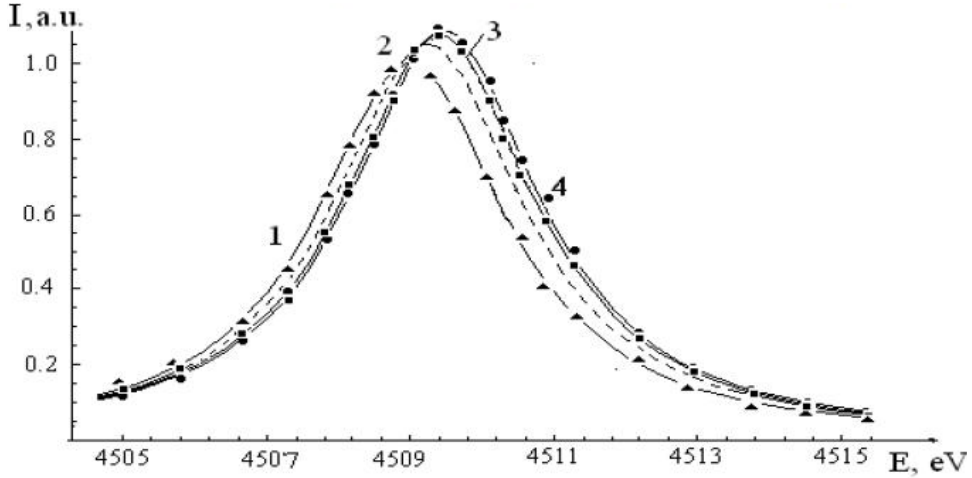

Figure 8 : Ti$K_{\alpha 1}$ X ray line profile in SrTiO3 samples: 1 – super pure, 2 - $SrTiO_3$: Mn, 3 - «blue spot» and $SrTiO_3$: Nd initial sample , 4 - $SrTiO_3$: Nd over plasma flow

spectra and growing concentration of Ti^{+3} ions in the samples. Ti^{+3} ion's relative concentration was calculated for selected samples: $C(Ti^{+3})$= (18 ± 6) % for entering Mn samples and $C(Ti^{+3})$ = (28 ± 6) and $C(Ti^{+3})$ = (32 ± 6) % for doping Nd samples before and after plasma treatment.

The shift in Sr$K_{\alpha 1}$ line for any crystal was less then experimental error.

There is important, relative intensity of Ti$K_{\alpha 1}$ line grows together with increasing VS on background of stability in Sr$K_{\alpha 1}$ line profile position. During experiments change in relative intensity of Ti$K_{\alpha 1}$ and Sr$K_{\alpha 1}$ lines and ratio $\kappa = I_{Sr}/I_{Ti}$ in the X ray lines intensities was detected, too. κ magnitude varies from 1.00 to 0.95 and 0.76 (0.73) for the perfect sample, entering Ni or Nd and "blue spot", respectively, in close agreement with data of the crystal density measurements[25].

Cr ions in ruby

Follow[14, 28 – 29] irradiation of sapphire and garnet crystals doped with Me ions creates the shift in Me$K_{\alpha 1}$ line, too. Upon irradiation we observe an increasing or decreasing ion oxidation state. γ- irradiation of ruby or garnet doped with Cr ions affects in a negative shift in Cr$K_{\alpha 1}$ X ray line. Theoretical VS value for Cr$K_{\alpha 1}$ line over increasing valence is following: $\Delta E(Cr^{3+} \rightarrow Cr^{4+})$ = - 1.20 eV. Metallic Cr sample was used as standard during experimental study of energy position and profile of Cr$K_{\alpha 1}$ line. Mathematical processing of X ray line profile (Lorentz's function) permits to evaluate VS as $\Delta E(CrK_{\alpha 1})$ = - (0.36 ± 0.08) eV. Follow theoretical and experimental data[1, 7, 29] negative X ray line shift corresponds to increasing oxidation state in every Me or RE ion.

Ab initio theory for clusters and solids

Follow[1, 14, 29] ab initio approach as symbiosis of the Hartree-Fock-Pauli method and the Heitler-London model was performed to study the electronic structure of clusters and doped crystals. Calculated and experimental parameters were compared for optical and X ray line spectra in Me and RE ions in selected wide band gap crystals.

The foundation of the theory is the well known Born-Oppenheimer approximation for unrestricted Me^{n+}: $[L]_k$ cluster where Me ion is encircled by k – neighborhoods ions - ligands (L). For the electronic part of the total wave function of a crystal, we can write the following equation:

$$\left[-\frac{1}{2}\sum_i \Delta_i - \sum_i V(r_i,R) + \sum_{i<j}\frac{1}{r_{ij}}\right]\Psi_l(r,R) = W_l(R)\Psi_l(r,R) \quad \textbf{(1)}$$

For Me/RE ion Eq.(1) may be written shortly as:

$$\left[H_{free}(r) + H_{\text{int}}(r,R)\right]\Psi_l(r,R) = E_l(R)\Psi_l(r,R) \quad \textbf{(2)}$$

where H_{free} is the Hamiltonian for the free ion and H_{int} describes electron–ion and electron-electron interactions. For the first step, we considering electronic structure of Me^{n+}:$[L]_k$ cluster, consisting in central Me ion with nl^N ground configuration surrounded by k ligands, at a distance R.

Using the one-electron approximation for the wave functions in the central field approximation, the energy of the cluster may be written as:

$$E(Me^{+n}:[L]_k) = E_0 + kE_1 + k'(E_Z + E_c + E_{ex}) \quad \textbf{(3)}$$

where E_0 (E_1) is the energy of the central ion and ligand respectively, in the free state.

The terms E_z, E_c and E_{ex} in Eq. (3) correspond to the energy of the interaction of electrons with the strange nucleus, the Coulomb interaction and the exchange interaction for all electrons. k', is a numerical coefficient depending on the symmetry of the cluster. Expressions for the terms E_z, E_c and E_{ex} in Eq. (3) written in[1, 4, 14].

The central field approximation where the one-electron wave function is determined as: $\phi_{nlm}(r,\theta,\varphi) = P(nl|r)Y_{lm}(\theta,\varphi)$ was taken into account. The system of equations for the radial functions of the Me/RE ion, $P(nl|r)$ and the ligand, $P(n'l'|r)$ was found as result of minimization of Eq. (3) with respect to the radial wave functions of the Me/RE ion and ligands.

The following system of equations may be written for each ion in the cluster:

$$\left[\frac{d^2}{dr^2} + \frac{2}{r}Y'(nl|r) - \varepsilon_{nl} - \frac{l(l+1)}{r^2}\right]P(nl|r) = X'(nl|r) + \sum_{n\neq n}\varepsilon_{n'l}P(n'l|r), \quad \textbf{(4)}$$

where ε_{nl} is one-electron energy. The Coulomb and exchange potentials, $Y'(nl|r)$ and $X'(nl|r)$ differ from

Review

the original Hartree-Fock potentials by the following additional terms.

$$\Delta Y(nl\,|\,r) = r/2\sum_{k,k_1,n'l'}[a_{ll'}^{kk_1}Y_{kk_1}(n'l',n'l'\,|\,r) + b_{ll'}^{kk_1}Y_{kk_1}(nl,n'l'|\,r)], \quad \textbf{(5)}$$

$$\Delta X(nl\,|\,r) = -\sum_{k,k_1,n'l'}[\alpha_{ll'}^{kk_1}Y_{kk_1}(nl,n'l'\,|\,r) + \beta_{ll'}^{k}r^{k_1}]P(n'l'\,|\,r),$$

Eqs. (5) describe the self-consistent field of the cluster depending on the state of each electron in the system. The tensor function, $Y_{kk1}(nl,n'l'|r)$ and coefficients: $a_{ll'}^{kk_1}$, $b_{ll'}^{kk_1}$, $\alpha_{ll'}^{kk_1}$, β^k are given in[14].

The energy of definite Stark-levels in crystalline field for Me/RE ion may be written as:

$$E(nl^N\,|\,\alpha\alpha' LSJ\Gamma) = E_0 + \sum_k f_k(l^N,\alpha\alpha' LS)F_k(nl,nl) +$$
$$+\chi(LSL'S',J)\eta(nl) + \sum_{k,q,i}B_{kq}Y_{kq}(\Theta_i\Phi_i), \quad \textbf{(6)}$$

where E_0, is the center of gravity of nl^N- configuration, $F_k(nl,nl$, the Slater's integrals, $\eta(nl)$, the spin-orbit constant, and B_{kq}, the crystal field parameters for RE or B, C and *Dq* for Me ion (TABLE 1) in a cubic field. The standard expression for radial integrals was used.

Follow[1, 4, 14, 29] the Eqs.1 – 6 are describing the radial distribution in the cluster electronic density and create possibility to study the change in ion electronic distribution during the transfer of the free Me/RE ion into the crystal, etc.

Selected experimental and theoretical parameters for energy levels in Cr^{+3} ions in the clusters are given in TABLE 1.

DISCUSSION

Plasma as powerful energy source changes the crystal surface morphology more effectively through energy absorption in near-surface layer with thickness nearby 10^{-6}- 10^{-7} m when melting in near-surface layers is possible. Simulation of surface structure transformation opens the main conditions for appearance of ordered nanostructures and change in surface properties such as, conductivity, melting temperature, scattering, etc.

Amorphous near surface layers were discovered in the sapphire when polycrystalline surface structure in the STO crystals was recorded. Appearance of destroyed layers accompanies by changing stoichiometry composition and high efficiency evaporation of strontium oxide in the STO samples. Deep change in stoichiometry relation was detected in the STO sample surface and we are waiting for similar and more week changes in sapphire. Variation in stoichiometry composition is basis for change in ground properties of oxides and creates powerful opportunities for applications.

One or two level nanostructures containing the systems of ordered and quasi-ordered unit crystallites like pyramid or needle type with size varying in range h = 10^{-7} - 10^{-10} m were found on the surface of the examined oxides. Notice, no connection in the SEM and AFM images and concentration of point defects in the oxides was found. Naturally, detail study of ordered nanostructures on the oxide surface needs for novel investigation. Simulation of charge distribution on the STO treated surface shows higher concentration of Ti^{+3} in pyramids peak and appearance of nano-ordered electric field.

Data of studying the X ray fluorescence lines shift and change in intensity of the Ti$K_{\alpha1}$ and Sr$K_{\alpha1}$ lines in the STO samples as perfect, un-doped or doped with Me or RE ions show a change in energy in the Ti$K_{\alpha1}$ line and magnitude of C_{Ti}/C_{Sr} ratio. Similar variation was observed in pure samples with yellow and "blue spot" parts and in the crystals doped with RE ions. No doubt in oxidation state change in some part of the Ti^{+4} ions into Ti^{+3} state and rising oxygen vacancy concentrations. As result, diminishing crystalline cubic parameter up *a* = (3.9052 ± 0.0008) Å to *a* = (3.8922± 0.0006) Å was found in STO perfect samples.

TABLE 1 : Theoretical and semi-empirical and data for parameters B, C and Dq for Cr^{+3} ion in selected oxides (cm^{-1})

Integral	Cr^{+3}: $[O^{-2}]_6$	α – Al_2O_3	$Y_3Al_5O_{12}$	$Gd_3Sc_5O_{12}$	$Gd_3Sc_2Ga_3O_{12}$
B	789	682	725	740	740
C	2829	3120	3373	3578	3578
Dq	1750	1787	1650	1500	1500

Review

Optical absorption band in the STO samples peaking at $\lambda = 620$ nm, luminescence one at $\lambda = 650$ nm and cathode-luminescence one nearby $\lambda = 700$ nm corresponds to transitions in different colour centres consisting the Ti^{+3} ions. Cathode-luminescence band intensity nearby $\lambda = 700$ nm in the "yellow" part grows closely to increasing probability in 3d $\leftrightarrow$ 3d transition in the Ti^{+3} ions surrounding by two oxygen's vacancies (Ti^{+3} in tetragonal symmetry environment). Stability of both centres can be related to the high magnitude of the STO dielectric constant.

Follow[14 - 16] optical absorption band peaked at $\lambda = 420$ nm registered in un-doped and the doped STO samples relating 3d $\rightarrow$ 4s transition in Ti^{+3} ions occupied, first of all, cubic sites. Cathode-luminescence band peaked at 450 nm (Figure 4) corresponding this defect, too. Comparison in the experimental and theoretical data shows that absorption band peaked at $\lambda = 520$ nm and cathode-luminescence one at $\lambda = 550$ nm determined by transitions in oxygen's vacancies trapped electron (so-called F-centre[5]). Strong dipole component of crystalline lattice appears in rising dichroism at $\lambda = 600 - 650$ nm was recorded in[25].

Exemplary, AA bands in the irradiated or plasma treated oxides have been observed at $\lambda = 217$, 360 and 460 nm in ruby and determined as electron's transition in Cr^{+4}: $[O^{2-}]_6$ clusters. Notice Cr^{+4} ions were registered in tetra-site of the YAG and complex garnets[9], too.

CONCLUSION

The findings of the experiments and their analysis make it possible to draw some conclusions and make suggestions about the main properties of the tested oxides. It was concluded that variation in growth conditions leads to change in crystals properties in particular appearance of radiation stimulated color centres. Appearance of ordered and quasi-ordered nanostructures with size of about 10^{-7}- 10^{-10} m were fitted on surface the plasma treated STO and sapphire. SEM or AFM images depend on relative position of tested sample area and plasma beam parameters. One-level nanostructures were found on surface for every tested sample when two-level sub-nanostructures were preliminary studied on the STO crystal surface.

Studying of treated samples permits to record the ordered systems of sub-nanostructures with size of about $10^{-9} - 10^{-10}$ m created on the surface of pure and doped STO, sapphire samples over plasma flow with dose at $W = (1 - 40)$ J·cm^{-2}.

Near surface layer is polycrystalline for the STO samples and amorphous for sapphire ones. Pyramid-like unit crystallites for the STO and needle like ones for sapphire were recorded, too. Plasma flow affects in evaporation of strontium oxide in STO and aluminium oxide in sapphire, accompanied by growth of oxygen's vacancy concentration and change in oxidation state of host and impurity ions. As an example of the STO crystal we can see how variation in stoichiometric relation moves to diminishing crystalline lattice parameters and change in the crystal optical spectra. Transparency, yellow and blue colour parts of the STO sample brightly show possibility for change in crystalline structure and crystal ground properties.

Strongly rising cathode-luminescence band at $\lambda = 700$ nm in in the STO sample (Figure 4) is the next good example for wide areas applications. Change in luminescence peaks intensity is mark of different type of' corresponding colour centres in the STO. Electronic structures of the centres determine different cross-section dispersion in clusters including Ti ion in different crystallographic sites[15, 16]. Gigantic growth of the peak intensity of cathode-luminescence at $\lambda = 700$ nm opened other way for luminescence stimulation through resonance processes interaction in Ti^{+3}: $[O^{-2}]_k$ centres and electron's beam in the STO crystals.

ACKNOWLEDGEMENTS

Author very grateful all colleagues and partners and first of all Dr. E. Hieckmann from TU Dresden, Prof. A. Konstantinova from Institute of Crystallography RAS, Moscow, Dr. L.A. Goroshova from Zaporozhye State University, Dr. I. Doichinovic from Centre Plasma in Belgrade, Prof. J. Dojcilovic from Belgrade University and Dr. A. Sandulenko from S.-Petersburg University for help in study of spectral

Review

properties and nano-structures in oxide photonic single crystals.

REFERENCES

[1] N.A.Kulagin, D.T.Sviridov; Methods of calculation of electronic structure of free and impurity ions, Nauka, Moscow, **(1986)**.

[2] A.N.Men, Ju.P.Vorob'ev, G.I.Chufanov; Physical-chemical properties of non-stoichiometrical oxides, Nauka, Leningrad, **(1973)**.

[3] A.Abragam, B.Bleaney; Electron paramagnetic resonance of transition ions, Claredon Press, Oxford, **(1970)**.

[4] N.A.Kulagin, D.T.Sviridov; Introduction to doped crystals physics, High School Publ., Kharkov, **(1990)**.

[5] H.Bartram, C.F.Swenbeg, J.T.Fournier; Theory of trapped-hole centers in aluminum oxide Phys.Rev., **139**, 941–966 **(1965)**.

[6] N.A.Kulagin; Radiative olor centers in doped sapphire crystals, Opt.Spectr., **101**, 402–409 **(2006)**.

[7] N.A.Kulagin, D.T.Sviridov; The spectra of chrome ions and irradiation influence on ruby, J.Phys.(L).C, **17**, 4539-4548 **(1984)**.

[8] N.A.Kulagin, E.Hieckamnn, J.Dojcilovic; Quasi-ordered nanostructures on the surface of strontium titanate, Phys.Stat.Sol., **52**, 2583-2592 **(2010)**.

[9] L.V.Krutova, N.A.Kulagin, V.A.Sandulenko, A.V.Sandulenko; Electronic states and positions of chromium ions in garnet crystals, Phys.Sol.Stat., **31**, 170-178 **(1989)**.

[10] N.A.Kulagin; Colour centers and nanostructures on the surface of laser crystals, Quant.Elects., **42**, 1008-1021 **(2012)**.

[11] N.A.Kulagin; Ab initio calculation and spectral properties of nano- and bulk materials, Cryst.Reps., **58**, 180-198 **(2013)**.

[12] T.S.Bessonova; Radiation stimulated processes in corundum single crystals, Probl.Nucl.Phys., **16**, 3-16 **(1982)**.

[13] N.A.Kulagin; Mixed valence of the rare earth and actinium ions in solid states, J.Alloys and Comps., **300-301**, 348-354 **(2000)**.

[14] Physics on Laser Crystals, Eds.J.C.Krupa, N.A.Kulagin, Kluwer Academic Publisher, Brussels, **(2003)**.

[15] N.A.Kulagin, L.A.Goroshkova, E.Hieckmann; Change in properties of nano and bulk $SrTiO_3$ crystals, Can.J.Phys., **90**, 683-691 **(2012)**.

[16] N.A.Kulagin, E.Hieckmann; Spectra and color centers in strontium titanate crystals, Opt.Spectr., **112**, 79-86 **(2012)**.

[17] N.A.Kulagin, J.Dojcilovic, E.Hieckmann; Nanostructures on surface of oxide single crystals treated by plasma, Mat.Sci.Appl., **2**, 971-976 **(2011)**.

[18] N.A.Kulagin, A.A.Levin, E.Langer, D.Meyer, I.Doichinovic, J.Puric; Formation of quasi ordered structures in field of plasma flow, Crystal.Reps., **53**, 1061-1967 **(2008)**.

[19] E.V.Zharikov, V.V.Osiko, I.A.Sherbakov; Izv.AS USSR.Seria fizika, **48**, 1330-1335 **(1984)**.

[20] N.V.Karlov, A.A.Manenkov; Quantum Amplifiers, Nauka, Moscow, **(1966)**.

[21] A.A.Kaminsky; Laser Crystals, Nauka, Moscow, **(1975)**.

[22] N.A.Kulagin; Structural, Doped, Radiation defects and properties of non-stoichiometrical solids, J.Mat.Sci.Forum, **494**, 55-59 **(2005)**.

[23] N.A.Kulagin, A.E.Ovechkin, E.A.Antonov; Investigation of the colour centres in γ-irradiated crystals, J.Appl .Spectr., **43**, 478-481 **(1985)**.

[24] N.A.Kulagin, M.F.Ozerov; Electronic states of Ti^{+3} ions in $SrTO_x$ and TiO_y single crystals, Phys.Stat.Sol., **35**, 2472 – 2480 **(1993)**.

[25] L.A.Korostel, E.V.Zhabotinskiy, A.F.Konstantinova, V.A.Sandulenko, N.A.Kulagin; Investigation of change of defects structure of strontium titanate under 77 K by optical methods, Crystal.Rep., **39**, 1092 -1096 **(1994)**.

[26] A.I.Morozov; Principels of coaxial (quasi-) steady-state plasma accelarators, Sov.J.Plasma Phys., **1**, 95-101 **(1975)**.

[27] M.M.Kuraica, V.M.Astashinski, I.P.Dojcinovic, J.Puric; Modification of solid surface by a compression plasma flow, in: J.-C.Krupa, N.A.Kulagin (Eds.), Physics of Laser Crystals, Kluwer Academic Publisher, Bruxelles, **(2003)**.

[28] N.A.Kulagin; Structure and dynamics of ordered clusters with ME or RE ions on oxide surface, J.Lumin., **131**, 526-531 **(2011)**.

[29] N.A.Kulagin; Electronic structure of clusters in ferroelectrics, Ferroelectr., **155**, 143-145 **(1994)**.